

## PAPER

## Calculation of impulse responses and acoustic parameters in a hall by the finite-difference time-domain method

Shinichi Sakamoto<sup>1,\*</sup>, Hiroshi Nagatomo<sup>2</sup>, Ayumi Ushiyama<sup>3</sup> and Hideki Tachibana<sup>4</sup>

<sup>1</sup>*Institute of Industrial Science, the University of Tokyo,  
4-6-1, Komaba, Meguro-ku, Tokyo, 153-8505 Japan*

<sup>2</sup>*Brüel & Kjær Division of Spectris Co., Ltd., Japan,  
1-8-11 Kitashinagawa, Shinagawa-ku, Tokyo, 140-0001 Japan*

<sup>3</sup>*Daiwa house industry Co., Ltd.,  
6-6-2 Sakyo, Nara, 631-0801 Japan*

<sup>4</sup>*Chiba Institute of Technology,  
2-17-1 Tsudanuma, Narashino, 275-0016 Japan*

(Received 27 July 2007, Accepted for publication 1 February 2008)

**Abstract:** Impulse responses in a hall were calculated by the finite-difference time-domain (FDTD) method, and typical room acoustic parameters were obtained from the responses. The calculated parameters were compared with those actually measured in the hall. In the FDTD calculation, the impedance boundary condition was modeled by an equivalent mechanical system comprising masses, springs, and dampers. To calculate the impulse responses, the normal acoustic impedance of the interior finishing materials of the various surfaces in the hall were measured by applying the impedance-tube method, and the model of the room boundary condition was determined for the respective parts. A comparison between the calculated and measured values showed that the values of reverberation time  $RT$ , definition  $D_{50}$ , clarity  $C_{80}$ , and center time  $T_s$  were in good agreement in the middle-frequency bands. However, in low-frequency bands, large discrepancies were observed because of the difficulties in determining and modeling the boundary conditions.

**Keywords:** Finite-difference time-domain method, Impulse response, Acoustic parameters

**PACS number:** 43.55.Br, 43.55.Ka [doi:10.1250/ast.29.256]

### 1. INTRODUCTION

In recent years, several wave-based numerical analysis methods have been developed, and they are being widely applied to various types of acoustic problems. Heretofore, in room acoustics, because of the limitations of computing power, geometry-based numerical methods represented by ray-tracing, cone-tracing, and image-source methods were developed and applied to the sound field analysis of rooms with large spaces. However, recently, the efficiency of computers has significantly increased and computation cost has been considerably reduced. Furthermore, advanced high-efficiency, high-speed calculation methods are being developed in accordance with the progress in of hardware technologies [1–4]. Under such circumstances, it is becoming feasible to apply wave-based numerical analysis methods to room acoustics. Among the numerical methods, the authors have been investigating the application of the

finite-difference time-domain (FDTD) method to room acoustics and outdoor sound prediction [5–7]. In this study, room impulse responses in a real hall with a volume of  $1,600\text{ m}^3$  were calculated by the FDTD method. In a preceding study on estimating impulse responses in a real hall using a wave-based numerical analysis, Yokota *et al.* carried out the FDTD analysis for a small concert hall and compared the calculation results with *in-situ* measurement results [8]. In their research, the absorbing boundary condition of the room surfaces was roughly dealt with by a single value of normal absorption coefficient for each part of the surface. In order to deal with the absorbing boundary condition in a real hall more precisely, in this study, a mechanical equivalent impedance model in which the boundary condition is modeled by an equivalent system comprising masses, springs, and dampers was applied. Here, the numerical system parameters of the masses, stiffness and resistance of the mechanical equivalent impedance model were determined from the normal acoustic impedance data actually measured for the interior

\*e-mail: sakamo@iis.u-tokyo.ac.jp

finishing materials used in the hall; the measurement was performed by the impedance-tube method. From the calculated impulse responses, the representative room acoustic parameters—reverberation time  $RT$ , definition  $D_{50}$ , clarity  $C_{80}$ , and center-time  $T_S$ —were calculated and compared with the measurements obtained in the real hall.

## 2. CALCULATION OF ROOM IMPULSE RESPONSES BY FDTD METHOD

### 2.1. Basic Equations

Under the assumption that air is completely at rest and sound does not lose energy during its propagation, a sound wave in a three-dimensional (3D) field is expressed by the following partial differential equations.

$$\rho \cdot \partial u / \partial t + \partial p / \partial x = 0 \quad (1)$$

$$\rho \cdot \partial v / \partial t + \partial p / \partial y = 0 \quad (2)$$

$$\rho \cdot \partial w / \partial t + \partial p / \partial z = 0 \quad (3)$$

$$\partial p / \partial t + \kappa(\partial u / \partial x + \partial v / \partial y + \partial w / \partial z) = 0 \quad (4)$$

Here,  $p$  denotes the sound pressure;  $u$ ,  $v$ , and  $w$ , the particle velocities in rectangular coordinates;  $\rho$ , the density of air; and  $\kappa$ , the volume elasticity of air.

In the FDTD Yee algorithm, the differential terms in Eqs. (1) to (4) are transformed into discrete terms by adopting the staggered-grid system. In this study, each spatial differential term is approximated by a finite differ-

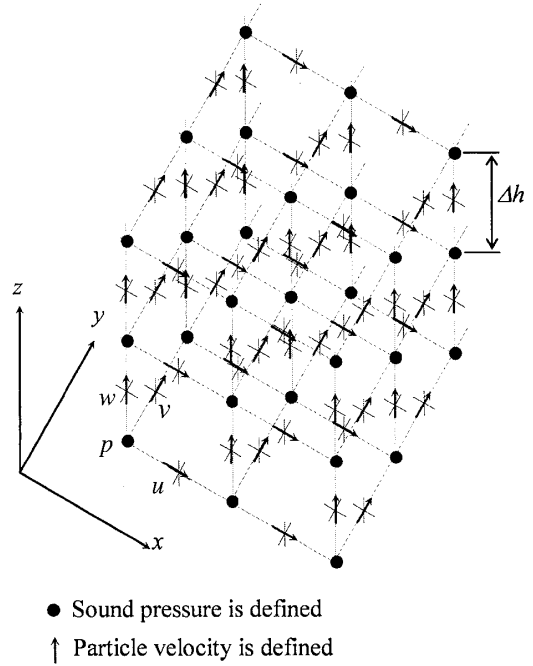


Fig. 1 3D staggered grid system used in the FDTD calculation.

ence with multiple reference points in order to improve the approximation accuracy. For example, a first-order spatial differential term of  $p$  in the  $x$ -direction at grid point  $x = a$  is approximated by the values at  $2M$  points in a staggered grid, as shown in the following equation [9].

$$\frac{\partial p(a)}{\partial x} = \sum_{m=0}^M \left\{ C_m / \sum_{l=0}^L (2l+1)C_l \right\} \left\{ \frac{p(a + (m+1/2)\Delta h) - p(a - (m+1/2)\Delta h)}{\Delta h} \right\} \quad (5)$$

$$C_m = (-1)^{m+1} \frac{(2M-1)^2(2M+1)^2}{\{2(M-m)+1\}^2} \frac{(2M+1)!}{m!(2M-m+1)!} \quad (6)$$

Here,  $\Delta h$  denotes the spatial interval of the reference points.

When applying Eq. (5) to a 3D sound field by adopting the staggered-grid system, as shown in Fig. 1, the discrete system equations for Eqs. (1) to (4) are expressed as

$$u^{n+1}(i+1/2, j, k) = u^n(i+1/2, j, k) - \frac{\Delta t}{\rho \Delta h} \sum_{m=0}^M D_m \{ p^{n+1/2}(i+m+1, j, k) - p^{n+1/2}(i-m, j, k) \} \quad (7)$$

$$v^{n+1}(i, j+1/2, k) = v^n(i, j+1/2, k) - \frac{\Delta t}{\rho \Delta h} \sum_{m=0}^M D_m \{ p^{n+1/2}(i, j+m+1, k) - p^{n+1/2}(i, j-m, k) \} \quad (8)$$

$$w^{n+1}(i, j, k+1/2) = w^n(i, j, k+1/2) - \frac{\Delta t}{\rho \Delta h} \sum_{m=0}^M D_m \{ p^{n+1/2}(i, j, k+m+1) - p^{n+1/2}(i, j, k-m) \} \quad (9)$$

$$p^{n+1/2}(i, j, k) = p^{n-1/2}(i, j, k) - \frac{\kappa \Delta t}{\Delta h} \left[ \sum_{m=0}^M D_m \{ u^n(i+m+1/2, j, k) - u^n(i-m-1/2, j, k) \} \right. \\ \left. + \sum_{m=0}^M D_m \{ v^n(i, j+m+1/2, k) - v^n(i, j-m-1/2, k) \} \right. \\ \left. + \sum_{m=0}^M D_m \{ w^n(i, j, k+m+1/2) - w^n(i, j, k-m-1/2) \} \right] \quad (10)$$

$$D_m = C_m \left/ \sum_{l=0}^L (2l+1)C_l \right. \quad (11)$$

## 2.2. Sound Source Condition

To simulate an impulsive sound source, a sound pressure distribution with a smooth profile, which is expressed by the following exponential function, was adopted as the initial condition for the calculation (see Fig. 2).

$$p(x, y, z) = \exp \left\{ -\frac{x^2 + y^2 + z^2}{(A\Delta h)^2} \right\} \quad (12)$$

Here,  $(x, y, z)$  is the set of relative coordinates of the grid point at which the center point of the impulse source is the origin;  $A$ , the coefficient that prescribes the width of the initial impulse source; and  $\Delta h$ , the discrete spatial grid size. In this study, the values selected for  $A$  and  $\Delta h$  were 3.0 and 0.06 m, respectively. Under these conditions, the impulse source possesses the spectral characteristic shown in Fig. 3; the spectral component increases with frequency up to approximately 1 kHz and then it falls steeply;

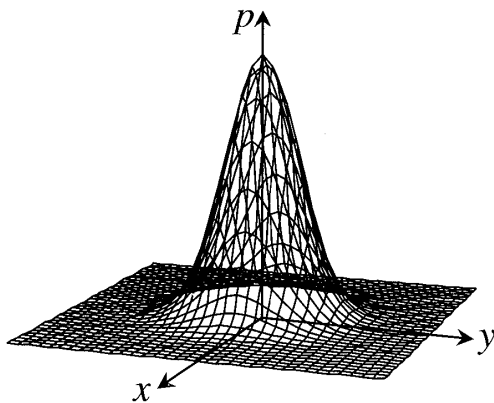


Fig. 2 Spatial sound pressure distribution of the impulse source used in this study.

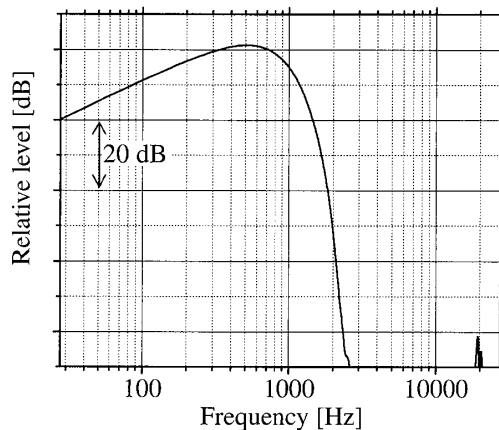


Fig. 3 Spectral characteristic of the impulse source used in this study ( $A = 3.0$  and  $\Delta h = 0.06$  m in Eq. (12)).

however, four octave bands at the center frequencies of 125 Hz, 250 Hz, 500 Hz, and 1 kHz, which are investigated in this study, are included in the spectral characteristic. To correct the spectral characteristic of the impulse source, the results calculated by the FDTD method were corrected by an inverse-filtering technique, as described below.

## 2.3. Correction of Spectral Characteristic of Impulse Source

To correct the spectral characteristic of the impulse source, first, a linear phase FIR band pass filter with a frequency range from 88 Hz to 1.414 kHz was designed. Figures 4(a) and (b) show the impulse response and spectral characteristic of this filter, respectively. The inverse filter required to correct the impulse response calculated using the impulse source was based on this filter and was obtained by a deconvolution operation, as shown in Figs. 5(a) and (b). By performing a convolution operation between the calculated impulse response and the impulse response of the inverse filter, the impulse response, under the assumption that the source has a flat spectral characteristic in the required frequency range, can be obtained.

## 2.4. Modeling of Impedance Boundary Condition

For the boundary condition in wave-based numerical analyses, the normal acoustic impedance of the boundaries is generally provided in a complex form and the reflection

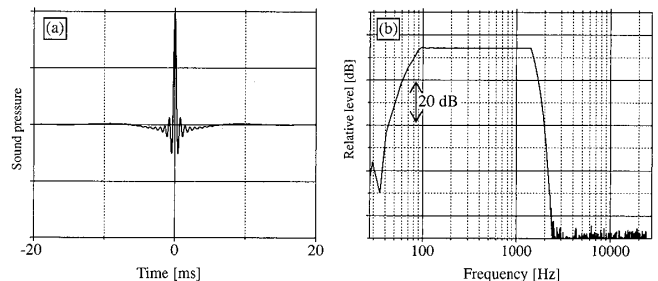


Fig. 4 Impulse response (a) and spectral characteristic (b) of the FIR band-pass filter for correcting the spectral characteristic of the impulse source used in this study.

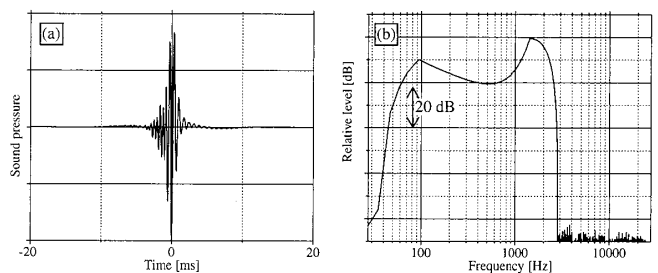


Fig. 5 Impulse response (a) and spectral characteristic (b) of the inverse filter.

at the boundaries is calculated under the assumption that local reactions occur. When using frequency-domain numeral techniques, such as the finite-element method (FEM) or boundary-element method (BEM), the characteristics of the frequency-dependent surface impedance can be directly reflected in the calculation by considering the value of surface impedance for the respective frequencies; on the other hand, in the case of the FDTD method, it is crucial to know how to deal with the frequency characteristics of the room boundaries. When the boundaries have a simple construction comprising porous material and air space, a relatively simple FDTD scheme is applicable, in which the sound absorption characteristic can be controlled by adjusting the acoustical parameters of the medium, such as density, sound speed, and flow resistance [10]. In this model, the physical parameters that affect sound absorption can be directly reflected in a numerical analysis, and therefore, the physical meaning is clear. However, in this method, the inner space of the absorbing wall must be divided into grid cells, and therefore, the required memory size increases. Chiba *et al.* have proposed another modeling method to simulate the boundary condition of finite impedance by applying an RCL electrical equivalent circuit [11]. This method has the advantage that a frequency-dependent normal impedance can be included in the FDTD calculations with a relatively small computer memory size. Similarly, in this study, the normal impedance is modeled by applying an equivalent mechanical system [12], as described in the next section. The impedance model adopted in this study is based on the same concept as the above method of applying the RCL circuit in the sense that the boundary is substituted with the other simple equivalent system, but the substituting systems are physically different each other.

(1) Modeling of normal acoustic impedance

A room surface with finite impedance is modeled using mechanical elements, mass, stiffness, and resistance, as shown in Fig. 6(a). For simplicity, this figure shows a one-dimensional (1D) sound field; mass  $m_1$  with area  $S$  is assumed to be moved by sound pressure  $p$ , which is applied to the surface of the mass. In this case, the momentum equation for the mass is expressed as

$$pS = m_1 \frac{\partial^2 x_1}{\partial t^2} + c_1 \frac{\partial x_1}{\partial t} + k_1 x_1. \tag{13}$$

Here,  $x_1$  is the displacement of mass  $m_1$ ;  $k_1$ , the stiffness of the spring; and  $c_1$ , the resistance coefficient of the mechanical system. To simplify the expression, the parameters included in Eq. (13) are normalized by the area  $S$ ; that is,  $m_1' = m_1/S$ ,  $k_1' = k_1/S$ ,  $c_1' = c_1/S$ :

$$p = m_1' \frac{\partial^2 x_1}{\partial t^2} + c_1' \frac{\partial x_1}{\partial t} + k_1' x_1. \tag{14}$$

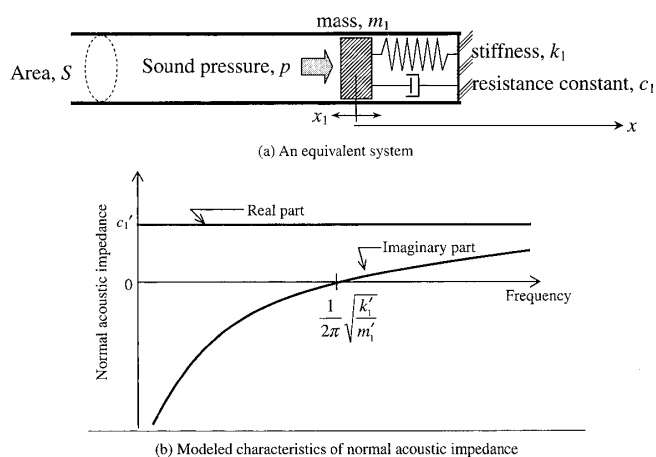


Fig. 6 Equivalent mechanical system with one degree of freedom simulating a room surface of finite impedance.

When dealing with a sinusoidal sound pressure of angular frequency  $\omega$ , Eq. (14) is transformed to:

$$p = (-m_1' \omega^2 + jc_1' \omega + k_1') x_1. \tag{15}$$

The relationship between particle velocity  $u_1$  and displacement  $x_1$  is expressed by Eq. (16) and the normal acoustic impedance  $z$  on mass  $m_1$  is expressed by Eq. (17).

$$u_1 = \frac{\partial x_1}{\partial t} = j\omega x_1 \tag{16}$$

$$z = \frac{p}{u_1} = c_1' + j \left\{ m_1' \omega - \frac{k_1'}{\omega} \right\} \tag{17}$$

In this case, the frequency characteristic of the normal acoustic impedance is relatively simple. As shown in Fig. 6(b), the real part of the modeled normal acoustic impedance has a constant value of  $c_1'$  and the imaginary part increases monotonically with increasing frequency. The normal acoustic impedance for many realistic room boundaries usually has more complicated frequency characteristics. Therefore, in order to cope with such a case, a more complicated equivalent mechanical system with two degrees of freedom, as shown in Fig. 7, is considered [12]. In this system, we have the following momentum equations.

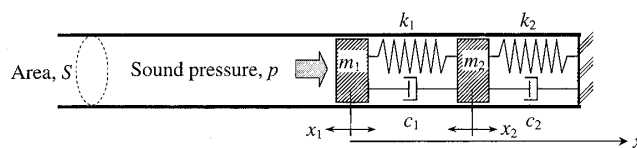


Fig. 7 Equivalent mechanical system with two degrees of freedom simulating a room surface of finite impedance.

$$p = m_1' \frac{\partial^2 x_1}{\partial t^2} + c_1' \frac{\partial x_1}{\partial t} + k_1'(x_1 - x_2) \quad (18)$$

$$k_1'(x_1 - x_2) = m_2' \frac{\partial^2 x_2}{\partial t^2} + c_2' \frac{\partial x_2}{\partial t} + k_2'x_2 \quad (19)$$

Here,  $x_1$  and  $x_2$  are the displacements of masses  $m_1$  and  $m_2$ , respectively. Here,  $m_1' = m_1/S$ ,  $m_2' = m_2/S$ ,  $k_1' = k_1/S$ ,  $k_2' = k_2/S$ ,  $c_1' = c_1/S$ , and  $c_2' = c_2/S$ .

When dealing with a sinusoidal sound pressure of angular frequency  $\omega$ , Eqs. (18) and (19) are transformed as follows:

$$p = (-m_1'\omega^2 + jc_1'\omega + k_1')x_1 - k_1'x_2 \quad (20)$$

$$k_1'x_1 = (-m_2'\omega^2 + jc_2'\omega + k_1' + k_2')x_2 \quad (21)$$

From Eqs. (16), (20), and (21), the following expression is obtained for the normal acoustic impedance.

$$z = \frac{p}{u_1} = c_1' + \frac{k_1'^2 c_2'}{\{-\omega^2 m_2' + (k_1' + k_2')\}^2 + \omega^2 c_2'^2} + j \left[ \left( \omega m_1' - \frac{k_1'}{\omega} \right) + \frac{(k_1')^2}{\omega} \frac{-\omega^2 m_2' + k_1' + k_2'}{\{-\omega^2 m_2' + k_1' + k_2'\}^2 + \omega^2 c_2'^2} \right] \quad (22)$$

The frequency characteristic of Eq. (22) is considerably more complicated in comparison to Eq. (17). This implies that a normal acoustic impedance with a complicated frequency characteristic can be simulated by properly selecting the values of parameters  $m_1'$ ,  $m_2'$ ,  $k_1'$ ,  $k_2'$ ,  $c_1'$ , and  $c_2'$ .

(2) FDTD calculation method adopting the impedance model

The impedance model obtained from the above-mentioned equivalent mechanical system with two degrees of freedom was adopted in the FDTD calculation scheme in this study. Figure 8 schematically shows the method for setting the mechanical system on a room surface of finite normal acoustic impedance. The figures are described in two dimensions for simplicity. For each grid cell ( $L, M, N$ ) on the room boundary having a normal vector  $(n_x, n_y, n_z)$ , one equivalent mechanical system is allotted and the displacements of the masses,  $x_{1,L,M,N}$  and  $x_{2,L,M,N}$ , are defined in the respective directions of the normal vector.

The momentum equations expressed by Eqs. (18) and (19) are transformed into discrete equations by using central finite differences, as follows:

$$P_{L,M,N}^{n+1/2} = m_1' \frac{x_{1,L,M,N}^{n+3/2} - 2x_{1,L,M,N}^{n+1/2} + x_{1,L,M,N}^{n-1/2}}{\Delta t^2} + c_1' \frac{x_{1,L,M,N}^{n+3/2} - x_{1,L,M,N}^{n-1/2}}{2\Delta t} + k_1'(x_{1,L,M,N}^{n+1/2} - x_{2,L,M,N}^{n+1/2}) \quad (23)$$

$$k_1'(x_{1,L,M,N}^{n+1/2} - x_{2,L,M,N}^{n+1/2}) = m_2' \frac{x_{2,L,M,N}^{n+3/2} - 2x_{2,L,M,N}^{n+1/2} + x_{2,L,M,N}^{n-1/2}}{\Delta t^2} + c_1' \frac{x_{2,L,M,N}^{n+3/2} - x_{2,L,M,N}^{n-1/2}}{2\Delta t} + k_2'x_{2,L,M,N}^{n+1/2} \quad (24)$$

From Eqs. (23) and (24), the displacements  $x_{1,L,M,N}$  and  $x_{2,L,M,N}$  are expressed as

$$x_{1,L,M,N}^{n+3/2} = \frac{\Delta t^2}{m_1' + c_1' \Delta t/2} P_{L,M,N}^{n+1/2} + \frac{2m_1' - k_1' \Delta t^2}{m_1' + c_1' \Delta t/2} x_{1,L,M,N}^{n+1/2} + \frac{-m_1' + c_1' \Delta t/2}{m_1' + c_1' \Delta t/2} x_{1,L,M,N}^{n-1/2} + \frac{k_1' \Delta t^2}{m_1' + c_1' \Delta t/2} x_{2,L,M,N}^{n+1/2} \quad (25)$$

$$x_{2,L,M,N}^{n+3/2} = \frac{k_1' \Delta t^2}{m_2' + c_1' \Delta t/2} x_{1,L,M,N}^{n+1/2} + \frac{2m_2' - (k_1' + k_2') \Delta t^2}{m_2' + c_1' \Delta t/2} x_{2,L,M,N}^{n+1/2} + \frac{-m_2' + c_1' \Delta t/2}{m_2' + c_1' \Delta t/2} x_{2,L,M,N}^{n-1/2} \quad (26)$$

The particle velocity in the normal direction of the surface at the time step of  $n + 1$ ,  $u_{nL,M,N}^{n+1}$ , is obtained by the central difference approximation from the displacements  $x_{1,L,M,N}$  at the time steps of  $n + 3/2$  and  $n + 1/2$ .

$$u_{nL,M,N}^{n+1} = \frac{x_{1,L,M,N}^{n+3/2} - x_{1,L,M,N}^{n+1/2}}{\Delta t} \quad (27)$$

The particle velocities,  $u_{L+1/2,M,N}^{n+1}$ ,  $v_{L,M+1/2,N}^{n+1}$ , and  $w_{L,M,N+1/2}^{n+1}$  are obtained as individual components in the  $x$ ,  $y$  and  $z$  directions of  $u_{nL,M,N}^{n+1}$ , respectively.

$$u_{L+1/2,M,N}^{n+1} = n_x \cdot u_{nL,M,N}^{n+1} \quad (28)$$

$$v_{L,M+1/2,N}^{n+1} = n_y \cdot u_{nL,M,N}^{n+1} \quad (29)$$

$$w_{L,M,N+1/2}^{n+1} = n_z \cdot u_{nL,M,N}^{n+1} \quad (30)$$

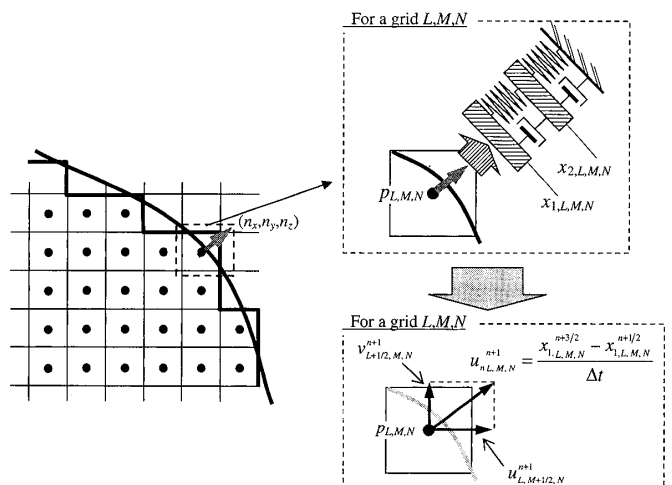


Fig. 8 Arrangement of the equivalent mechanical system on the room boundary.

### 3. COMPARISON OF RESULTS OF FDTD CALCULATION AND MEASUREMENTS

To examine the applicability of the FDTD calculation method with the impedance model, the impulse responses and major room acoustic parameters were calculated for a real hall. For this calculation, the normal acoustic impedance of the interior finishing materials used in the hall was measured by the impedance-tube method. The calculation results were compared with the measured results for the hall.

#### 3.1. Hall under Investigation and Discretization in FDTD Calculation

Figures 9(a) and 9(b) show the plan and cross section of the hall investigated in this study, respectively. The hall has a room volume of  $1,600\text{ m}^3$  and 257 audience seats. The entire surrounding wall is smoothly curved, and a sequence of sound diffusers with a triangular section are attached to the side walls. The sound field in this hall was discretized using the Cartesian grid system with grid size  $\Delta h = 0.06\text{ m}$ . The curved and oblique surfaces were approximated as zig-zag shapes. In reality, the entire surrounding wall is covered with aluminum ribs with dimensions of  $0.05\text{ m} \times 0.1\text{ m}$  at intervals of  $0.1\text{ m}$ ; however, these ribs were ignored in the calculation because their dimensions are too small compared with the grid size adopted in this study. Under these conditions, the room impulse responses from a sound source set on the stage at ten receiving points in the audience area were calculated.

#### 3.2. Characterization of Room Boundary Condition

To set the room boundary condition in the FDTD calculation, the normal acoustic impedance of each absorptive interior finishing material of the hall was measured. The samples of the materials used in different parts of the hall—the side and back walls, floor, ceiling, and several parts of the chairs—were preferred specimens (Fig. 9), and the normal acoustic impedance of each specimen was measured up to  $1,600\text{ Hz}$  by the impedance-tube method, using an impedance tube (BK 4206) with a diameter of  $100\text{ mm}$ , and the transfer-function method specified in ISO 10534-2. The measured values of the normal acoustic impedance and the normal incidence sound absorption coefficient for the different parts of the hall are shown by solid lines in Fig. 10.

On the basis of these measurement results, the parameters in the impedance model for the FDTD calculation— $m_1'$ ,  $m_2'$ ,  $c_1'$ ,  $c_2'$ ,  $k_1'$ , and  $k_2'$ —were determined for each material such that the frequency characteristic of the hypothetical normal acoustic impedance calculated by Eq. (22) and the normal sound absorption coefficients calculated from the normal acoustic impedance

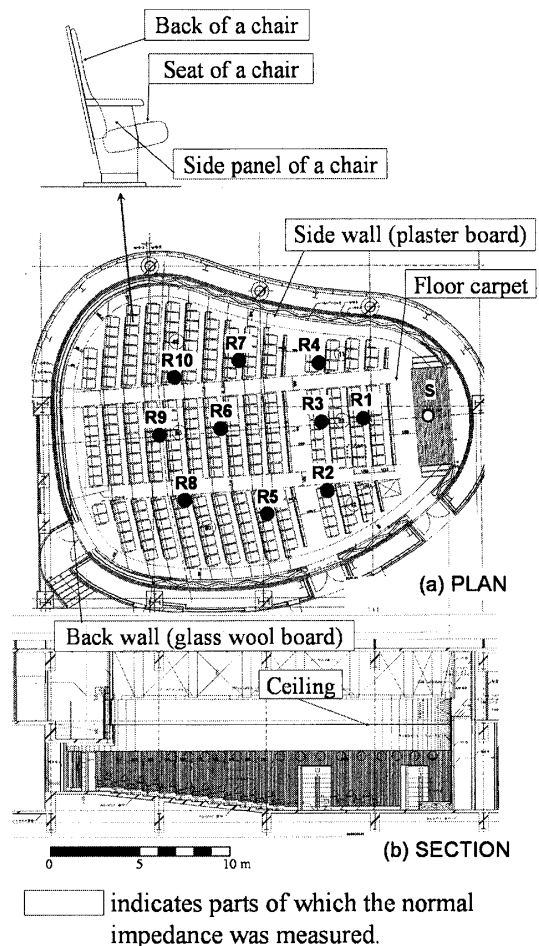


Fig. 9 Convention hall under investigation.

showed a good fit with the measurement results. The values of the respective parameters thus determined for each part and the modeled impedance and absorption coefficient characteristics are shown in Table 1 and in Fig. 10 (by dotted lines). As shown in the figures, the frequency characteristics of the normal acoustic impedance and sound absorption coefficient for the different parts could be roughly simulated by the impedance model. However, as shown in Figs. 10(c) and 10(g), at low frequencies, considerable differences are observed between the measured and the modeled characteristics of the normal acoustic impedance. These differences are caused by the mechanical elements owing to the limitation of the impedance model.

#### 3.3. Comparison of Calculated and Measured Impulse Responses and Acoustic Parameters

Band-limited impulse responses in the frequency range from  $88\text{ Hz}$  to  $1.414\text{ kHz}$ , which include four octave bands of  $125\text{ Hz}$ ,  $250\text{ Hz}$ ,  $500\text{ Hz}$ , and  $1\text{ kHz}$ , were obtained from the results of the FDTD calculation and the field measurement. In the field measurement, the impulse responses were measured in the hall for the same sound source and

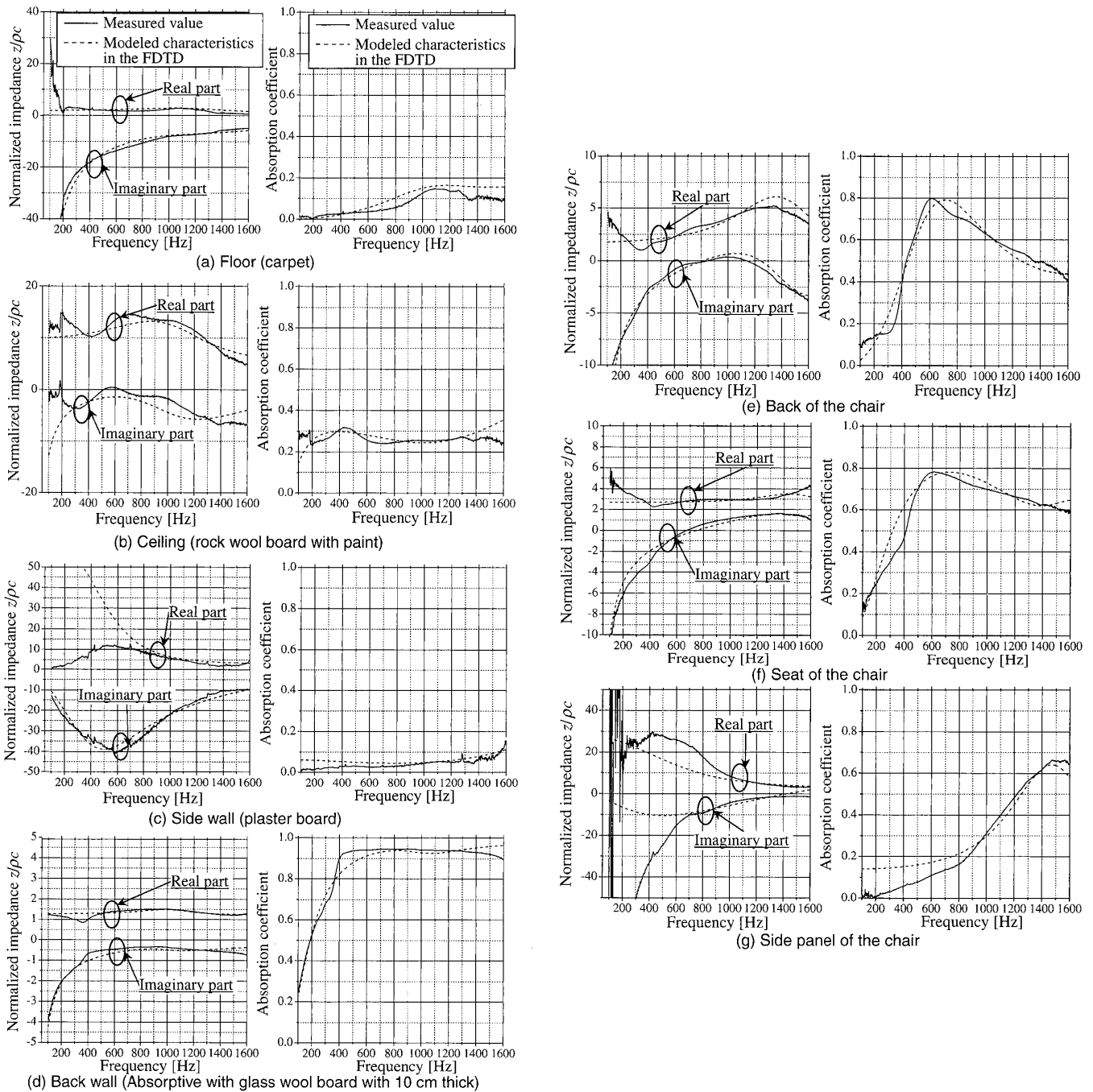


Fig. 10 Normal acoustic impedance and absorption coefficient of different parts of the boundary of the hall.

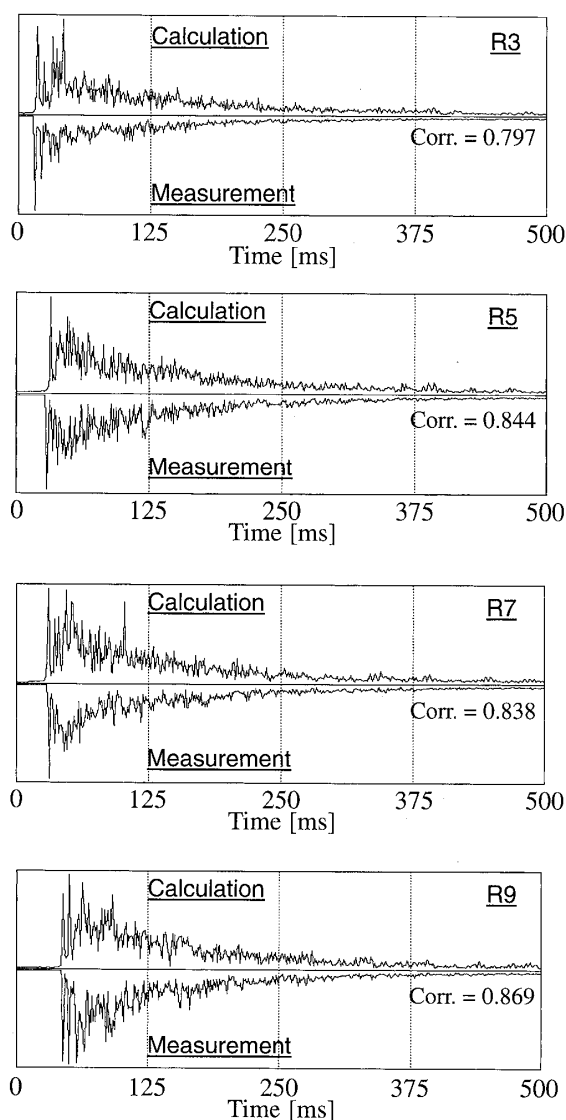
receiving positions by applying the swept-sine method. For this measurement, a dodecahedral loudspeaker was placed on the stage at a height of 1.5 m and a (1/2)-inch omnidirectional microphone was placed at each receiving point at a height of 1.2 m above the floor. Four examples of the comparison between the echo diagrams of the calculated and the measured values—front seat, R3; back seat; R9, middle seats, R5 and R7—are shown in Figs. 11(a) to (d). These echo diagrams were obtained by passing the impulse response signal through a numerical RMS detector with a time constant of 1 ms. In these figures, “Corr.”

means the cross-correlation coefficient between the echo diagrams of the calculated and measured values calculated for the range of 1 second of the responses. The coefficient is approximately 0.8 for all the results shown in Fig. 11. Similar tendencies were observed in the results obtained for the other receiving points.

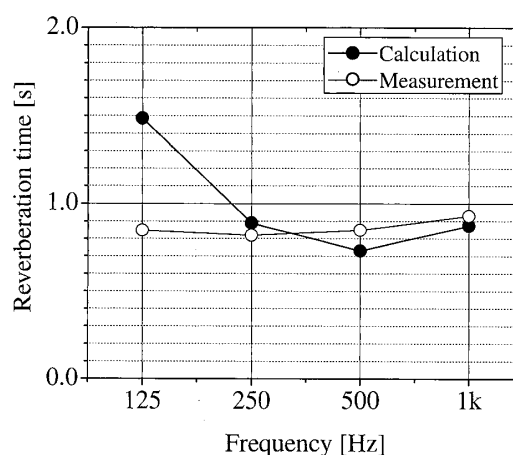
To further compare the impulse responses obtained by the FDTD calculation and the actual measurement more quantitatively, the major room acoustic parameters calculated from the impulse responses were compared. First, the reverberation time ( $RT$ ) in each octave band was calculated

**Table 1** Values of the parameters included in the impedance model for different parts of the boundaries.

	Part	$m'_1$	$c'_1$	$k'_1$	$m'_2$	$c'_2$	$k'_2$
1	Floor (carpet)	0.01	$4.0 \times 10^2$	$2.3 \times 10^7$	2.4	$1.35 \times 10^4$	$1.2 \times 10^8$
2	Ceiling (rock wool board with large air space)	0.1	$2.0 \times 10^3$	$2.0 \times 10^7$	0.5	$3.0 \times 10^3$	$4.0 \times 10^6$
3	Side wall (plaster board)	0.2	$1.0 \times 10^3$	$5.5 \times 10^7$	5.0	$2.5 \times 10^4$	$3.5 \times 10^5$
4	Rear wall (glass wool board with a thickness of 100 mm)	0.001	$5.0 \times 10^2$	$1.4 \times 10^6$	0.15	$4.5 \times 10^2$	$5.0 \times 10^6$
5	Back of the chair	0.07	$1.0 \times 10^2$	$1.5 \times 10^7$	0.25	$1.2 \times 10^3$	$6.0 \times 10^6$
6	Seat of the chair	0.11	$1.05 \times 10^3$	$4.0 \times 10^6$	0.15	$5.0 \times 10^2$	$9.0 \times 10^6$
7	Side panel of the chair	0.38	$1.0 \times 10^3$	$2.7 \times 10^7$	1.0	$1.0 \times 10^4$	$5.0 \times 10^3$
8	Rigid wall	$\infty$	0.0	0.0	$\infty$	0.0	0.0

**Fig. 11** Examples of comparisons of echo diagrams between the calculation and the measurement.

by the integrated impulse response method for all the receiving points and the results were averaged for each octave band. The results for the FDTD calculation and the

**Fig. 12** Calculated and measured reverberation times.

measurement are shown in Fig. 12. In this figure, it is observed that the calculated and measured values are in fairly good agreement in the 250 Hz, 500 Hz, and 1 kHz bands, whereas a large discrepancy is observed in the 125 Hz band. This discrepancy might be attributed to the setting of the boundary condition at low frequencies in the FDTD calculation. In other words, the sound absorption effects of panel vibration and Helmholtz resonance in the rib wall at low frequencies were not considered in the calculation because these effects cannot be measured by the impedance-tube method.

The other room acoustic parameters obtained from the impulse response—definition  $D_{50}$ ; clarity  $C_{80}$ ; and center time  $T_S$ —(specified in ISO 3382) were calculated for the frequency range including the two octave bands of 500 Hz and 1 kHz in order to reduce the interference effects [13,14]. For both FDTD calculation and measurement, the parameters were deduced from the impulse responses for 1 second. The FDTD calculations and the measured values of each of these parameters are shown in Figs. 13(a) to (c). Although some discrepancies are observed in the results of  $C_{80}$  at the receiving points R1, R4, R8, R9, and R10, the

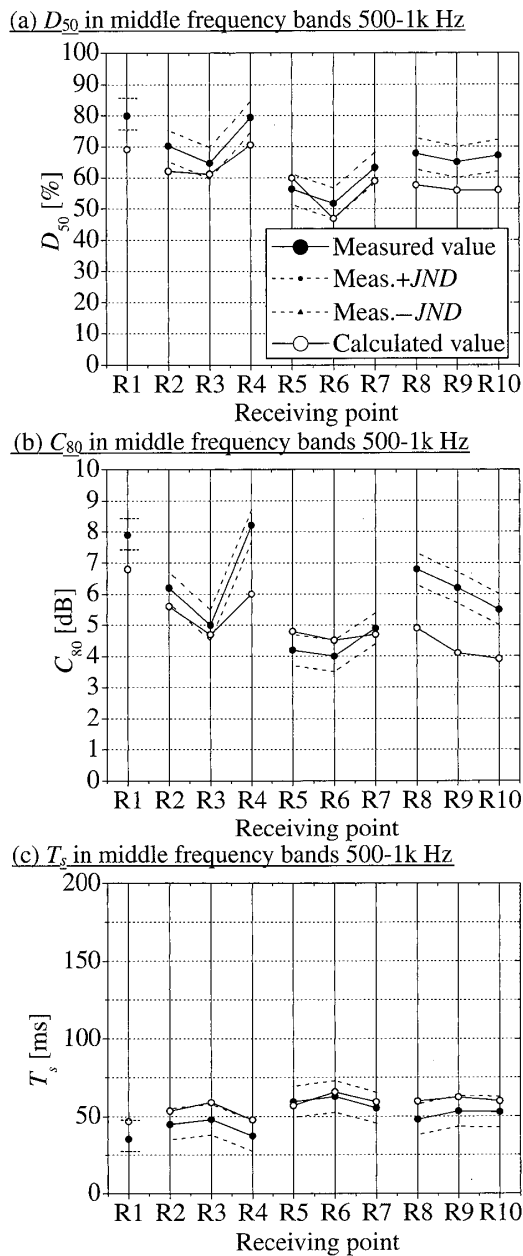


Fig. 13 Calculated and measured values of  $D_{50}$ ,  $C_{80}$ , and  $T_s$  in the middle-frequency range.

FDTD calculations and the measured values are in fairly good agreement on the whole. In the figures, the dotted lines indicate the range of the measured value  $\pm JND$  (just noticeable difference limen) [15].

#### 4. CONCLUSIONS

Since the FDTD numerical analysis method has an advantage over FEM and BEM when studying transient phenomena, the application of the FDTD Yee algorithm using the staggered-grid system for room acoustics has been investigated in this study. As the method of simulating the normal acoustic impedance of the room boundaries, an equivalent mechanical system with two degrees of freedom was adopted. To examine the applicability of this

FDTD method, the room impulse responses in a real hall were calculated using the normal acoustic impedance data of the different room surfaces of the hall, which were measured by the impedance-tube method. For the echo diagrams, reverberation time, and other major room acoustic parameters (definition  $D_{50}$ , clarity  $C_{80}$  and center time  $T_s$ ), the calculated values were compared with those actually measured in the hall. As a result, a fairly high correlation was found among the echo diagrams. The calculated and measured reverberation time were in good agreement in the middle-frequency range, whereas a big discrepancy was observed in the octave band at 125 Hz, at which the room boundary condition was not well simulated in the calculation. A fairly good agreement was obtained when the calculated and measured values of  $D_{50}$ ,  $C_{80}$ , and  $T_s$  were compared on the whole. From these results, it can be concluded that the room impulse response can be calculated well by the FDTD method introduced here if the normal acoustic impedance data of the room boundaries are available. However, the methods of simulating the sound absorption caused by panel vibration and resonance-type elements at low frequencies should be investigated in the future. Although the FDTD algorithm is advantageous with regard to computer memory size and computation time in comparison to other numerical analysis methods, the highest operational frequency in practical calculations is limited to one or several thousand Hz at present. The upper limit of this frequency must be raised in the future.

#### REFERENCES

- [1] N. Okamoto, T. Otsuru, R. Tomiku and T. Okuzono, "Performance of iterative methods and acceleration of computation for large-scale finite element sound field analysis in rooms," *Proc. The 9th Western Pacific Acoustics Conference*, Seoul, Korea (2006).
- [2] T. Otsuru, N. Okamoto, R. Tomiku, D. Azuma and K. Yamamura, "Large-scale finite element sound field analysis, design and scientific tool for room acoustics," *Proc. Inter-noise 2005*, Rio de Janeiro, Brazil (2005).
- [3] T. Sakuma and Y. Yasuda, "Fast multipole boundary element method for large-scale steady-state sound field analysis, Part I: Setup and validation," *Acta Acust. Acust.*, **88**, 513–525 (2002).
- [4] Y. Yasuda and T. Sakuma, "Fast multipole boundary element method for large-scale steady-state sound field analysis, Part II: Examination of numerical items," *Acta Acust. Acust.*, **89**, 28–38 (2003).
- [5] T. Yokota, S. Sakamoto and H. Tachibana, "Sound field simulation method by combining finite difference time domain calculation and multi-channel reproduction technique," *Acoust. Sci. & Tech.*, **25**, 15–23 (2004).
- [6] T. Yokota, S. Sakamoto and H. Tachibana, "Visualization of sound propagation and scattering in rooms," *Acoust. Sci. & Tech.*, **23**, 40–46 (2002).
- [7] S. Sakamoto, T. Seimiya and H. Tachibana, "Visualization of sound reflection and diffraction using finite difference time domain method," *Acoust. Sci. & Tech.*, **23**, 34–39 (2002).
- [8] T. Yokota, S. Sakamoto, H. Tachibana, M. Ikeda, K. Takahashi and T. Otsuru, "Comparison of room impulse response

S. SAKAMOTO *et al.*: CALCULATION OF IMPULSE RESPONSES IN A HALL BY THE FDTD METHOD

- calculated by the simulation methods based on geometrical acoustics and wave acoustics," *Proc. ICA 2004*, Vol. 4, pp. 2715–2716 (2004).
- [9] S. Sakamoto, "Phase-error analysis of high-order finite difference time domain scheme and its influence on calculation results of impulse response in closed sound field," *Acoust. Sci. & Tech.*, **28**, 295–309 (2007).
- [10] H. Suzuki, A. Omoto and K. Fujiwara, "Treatment of boundary conditions by finite difference time domain method," *Acoust. Sci. & Tech.*, **28**, 16–26 (2007).
- [11] O. Chiba, T. Kashiwa, H. Shimoda, S. Kagami and I. Fukai, "Analysis of sound fields in three dimensional space by the time-dependent finite-difference method based on the leap frog algorithm," *J. Acoust. Soc. Jpn. (J)*, **49**, 551–562 (1993) (in Japanese).
- [12] S. Sakamoto and H. Tachibana, "Calculation of impulse responses in 3-D sound field with absorptive boundary by the finite difference method," *Proc. inter-noise 97*, pp. 1597–1600 (1997).
- [13] M. Barron, "Using the standard on objective measures for concert auditoria, ISO 3382, to give reliable results," *Acoust. Sci. & Tech.*, **26**, 162–169 (2005).
- [14] J. S. Bradley, "Using ISO 3382 measures, and their extensions, to evaluate acoustical conditions in concert halls," *Acoust. Sci. & Tech.*, **26**, 170–178 (2005).
- [15] ISO/DIS 3382-1:2006 "Acoustics—Measurement of room acoustic parameters—Part 1: Performance rooms, Annex A Auditorium measures derived from impulse responses" (2006).